Effects of the annealing of amorphous Ta_2O_5 coatings produced by ion beam sputtering concerning the effusion of argon and the chemical composition

A. Paolone, E. Placidi, E. Stellino, M.G. Betti, E. Majorana, C. Mariani, A. Nucara, O. Palumbo, P. Postorino, I. Rago, et al.

Effects of the annealing of amorphous Ta_2O_5 coatings produced by ion beam sputtering concerning the effusion of argon and the chemical composition

A. Paolone, E. Placidi, E. Stellino, M.G. Betti, E. Majorana, C. Mariani, A. Nucara, O. Palumbo, P. Postorino, I. Rago, et al.

Effects of the annealing of amorphous Ta_2O_5 coatings produced by ion beam sputtering concerning the effusion of argon and the chemical composition

A. Paolone [a,b,*], E. Placidi [b,c], E. Stellino [d], M.G. Betti [b,c], E. Majorana [b,c], C. Mariani [b,c], A. Nucara [c], O. Palumbo [a], P. Postorino [c], I. Rago [b,c], F. Trequattrini [c], M. Granata [e], J. Teillon [e], D. Hofman [e], C. Michel [e], A. Lemaitre [f], N. Shcheblanov [f], G. Cagnoli [g], F. Ricci [b,c]

[a] *Consiglio Nazionale delle Ricerche, Istituto dei Sistemi Complessi, Piazzale A. Moro 5, I-00185 Roma, Italy*
[b] *Istituto Nazionale di Fisica Nucleare, Piazzale A. Moro 5, I-00185 Roma, Italy*
[c] *Sapienza Università di Roma, Dipartimento di Fisica, Piazzale A. Moro 5, I-00185 Roma, Italy*
[d] *Università di Perugia, Dipartimento di Fisica e Geologia, Via Pascoli, I-06123 Perugia, Italy*
[e] *Laboratoire des Matériaux Avancés – IP2I, CNRS, Université de Lyon, F-69622 Villeurbanne, France*
[f] *Laboratoire Navier, Ecole des Ponts, Univ. Gustave Eiffel, CNRS, F-77420 Marne-la-Vallée, France*
[g] *Université de Lyon, ENS de Lyon, Univ. Claude Bernard Lyon 1, CNRS, Laboratoire de Physique, F-69342 Lyon, France*

Keywords:
Amorphous tantala
Thermal treatments
Gravitational-wave detectors
Argon

A B S T R A C T

We investigate the effects of thermal treatments in vacuum or air on amorphous Ta_2O_5 deposited on crystalline Si by Ion Beam Sputtering, mimicking the coatings of the mirrors of the gravitational-wave revealers of the Advanced Virgo and Advanced LIGO detectors. Argon is present in the whole thickness of the coating, likely introduced during the synthesis, and it can be released above 200°C in vacuum, while less discharge of Ar is detected during heating in air. Formation of sub-stoichiometric Ta oxides is evidenced in the surface layers, after in-vacuum annealing. The macroscopic structure of the samples is not affected by the thermal treatments. However, the length of the interference fringes, due to the coating, decreases after thermal treatments both in air and in vacuum, suggesting an increase of the Ta_2O_5 thickness of ~1-2%, caused by an increase of the volume of the pores present in the structure.

1. Introduction

Amorphous Ta_2O_5 is a material with a large variety of applications in electronic circuits [1], quantum technologies [2], gas [3] or molecular sensing [4], enhancement of Raman scattering [5], hydrogen generation activity [6] or hydrophobic activity [7]. Among the physical properties which allow this broad range of applications, the refractive index n~2.1 at 1064 nm is of the highest importance [8]. Actually, multilayers reflecting coatings and photonic crystals are conceived and realized combining films of different refractive index in stacked sequences. This possibility has been largely explored for the construction of the coatings of the most demanding optical components ever realized: the mirrors of the gravitational-wave (GW) detectors [8–13]. At the present state, the mirrors of the Advanced Virgo and Advanced LIGO detectors are large masses of silica (35 cm diameter, 40 kg mass) with a high reflecting coating composed of alternate layers of amorphous SiO_2 and Ta_2O_5 [8, 14,15].

In this particular application, besides the optical properties, the most important parameter is the mechanical energy loss, because it is the key limiting factor of the interferometer performances due to the associated thermal noise [16]. Despite the small thickness of the coating (≤6 μm) compared to that of the bulk mirror (about 20 cm), the main source of mechanical energy loss is indeed the thin film, in particular the Ta_2O_5 layers [16]. Two principal strategies to reduce the coating loss have been proposed: doping with amorphous TiO_2 or post deposition thermal treatments [16,17]. In the following we will investigate in more detail some effects of the second procedure. Previous reports evidenced that Ta_2O_5 has a mechanical energy dissipation about 10 times higher than SiO_2 [16]. The exact value for Ta_2O_5 depends on the deposition technique; however, after a thermal treatment for 10 hours in air, the elastic

* Corresponding author.
E-mail address: annalisa.paolone@roma1.infn.it (A. Paolone).

https://doi.org/10.1016/j.jnoncrysol.2021.120651
Received 8 October 2020; Received in revised form 16 December 2020; Accepted 3 January 2021
Available online 3 February 2021

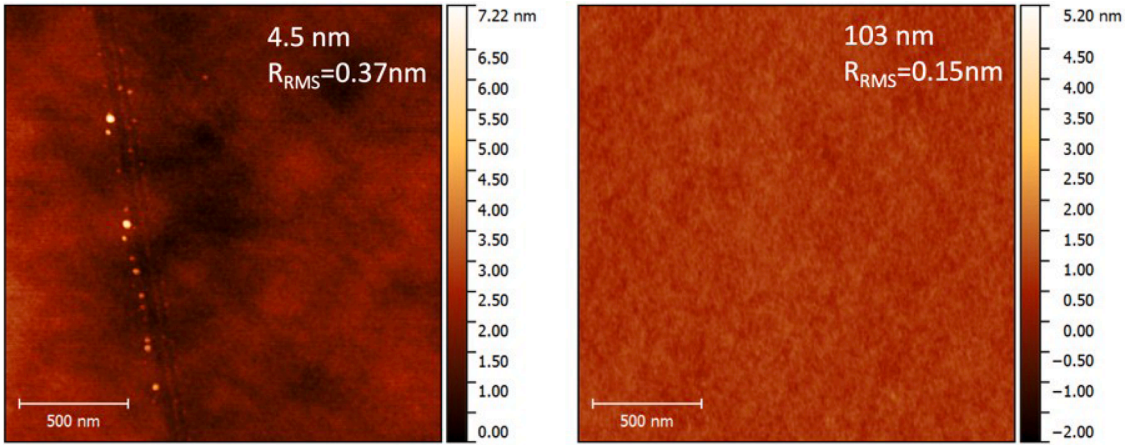

Fig. 1. AFM topographies of Ta_2O_5 layers with 4.5 nm (left panel) and 103 nm (right panel) coatings.

dissipation reduces and reaches the same value, independently of the synthesis method [16]. This procedure has been largely used for the production of the mirrors of the gravitational-wave detectors. Also the refractive index of Ta_2O_5 slightly depends on the synthesis method; however, the small differences seem not to be erased by thermal treatments [16]. Notably, longer thermal treatments do not have an impact either on the elastic loss or on the refractive index [8].

While the macroscopic effects produced on the optical and mechanical properties by the thermal treatments have been largely investigated, much less is known about the induced microscopic changes. An investigation of Ta_2O_5 by Extended X-ray Absorption Fine Structure (EXAFS) measurements evidenced that samples annealed in air at 300 and 600°C displayed only marginal changes of the amorphous structure, when it is investigated on a length scale of 50 nm [18]. These results are in agreement with Raman spectroscopy measurements that could not reveal important changes of the Ta_2O_5 structure on a macroscopic length scale induced by thermal treatments [8]. However, Fluctuation Electron Microscopy (FEM) measurements on Ion Beam Sputtered amorphous tantala coatings revealed a medium range order on a typical length scale of 2 nm; this spatial scale increases up to 5 nm in samples thermally treated at 600°C [19], even though a macroscopic crystallization is not revealed at this temperature.

In the present work, we further investigate the effects of thermal treatments on amorphous Ta_2O_5 produced by Ion Beam Sputtering (IBS), as this production technique is the method of choice to obtain the highly uniform coatings needed for gravitational-waves detectors [13]. Some aspects are deeply investigated: the first is the possible retain of argon atoms in the coating during the synthesis procedure. In fact, in the IBS deposition, an Ar ion beam is used to produce the sputtered matter to be deposited on the substrate and some atoms could be retained either at the coating/substrate interface or in the whole thickness of the film. Moreover, possible subtle changes of the stoichiometry of the coating surface after thermal treatments are investigated. Finally, the variation of refractive index or coating thickness after heating under different conditions is critically studied.

2. Experimental

The investigated samples consisted in amorphous Ta_2O_5 films deposited on crystalline Si wafers. They were produced at Laboratoire de Matériaux Avancés in Lyon by means of IBS in a VEECO Spector system. All coatings have been produced using accelerated, neutralized argon ions as sputtering particles. Argon was fed into the ion-beam sources while oxygen was fed into the chamber, for a total residual pressure inside the chamber of the order of 10^{-4} mbar. During deposition, the sputtered coating particles impinged on substrates heated up to about 100°C; the ion energy and current were of the order of 1 keV and 0.5 A, respectively. For the present study, four different thicknesses of the coatings were produced under the same conditions (4.5, 14, 103 and 953 nm) and a choice among them was performed for various spectroscopic studies, according to the desired information to be obtained.

Concomitant mass spectrometry and thermogravimetric (TGA) measurements were performed in a vacuum of the order of 10^{-5} mbar in a Setaram Setsys Evolution 1200 system coupled to a Pfeiffer Vacuum quadrupole mass spectrometer, used to detect the possible evolution of argon gas.[20] The choice to perform measurements in a vacuum was motivated by the much higher sensitivity of the mass spectrometer when working in a pressure lower than 10^{-2} mbar. Measurements were conducted between room temperature and 600°C with a temperature rate of ≈ 3°C/min on the "as deposited" samples. A specific sample holder was realized by means of a platinum wire able to sustain the large initial mass of samples, which was much higher than the usual one for TGA experiments (5 g in the present case vs. 10 mg).

Surface morphology was investigated ex situ by a VEECO multimode (Nanoscope IIIa) Atomic Force Microscopy (AFM) in the tapping mode by using nonconductive Si tips with a nominal radius of about 5-7 nm.

The X Ray Photoelectron Spectroscopy (XPS) experiments were carried out at the Nanostructures at Surfaces laboratory at Sapienza University in Rome, in an Ultra-High-Vacuum (UHV) chamber with a base pressure in the low 10^{-10} mbar range. An X-ray photon source with $h\nu$=1253.6 eV was used (PSP TA10 Mg Kα); photoelectrons were measured with a hemispherical VG Microtech Clam-2 electron analyzer in constant pass energy mode set at 50 eV and with overall energy resolution better than 1 eV. The binding energy (BE) scale was calibrated on a freshly sputtered gold foil in electrical contact with the sample, by setting the Au $4f_{7/2}$ core-level at 84.0 eV BE. XPS experiments were performed on the "as-deposited" samples and on small parts of the same samples heated either in vacuum at 300°C in situ or in air at 500°C for 10 hours (ex situ).

Mid-infrared reflectivity measurements were performed at ambient conditions using a commercial Bruker Interferometer coupled with an infrared microscope (Bruker Hyperion 2000) and a gold mirror as reference. For each sample, 25 different positions were considered, collecting spectra on an area of 5 × 5 mm^2 with steps of 1 mm in the two perpendicular directions. The incident light spot size was fixed at 200 μm. Spectra were collected with 4 cm^{-1} resolution and each spectrum was the average of 256 scans for each point. A nitrogen cooled mercury-cadmium-telluride (MCT) and a potassium bromide (KBr) crystal were used as detector and beamplitter, respectively.

Raman measurements have been performed at ambient conditions using a Horiba spectrometer equipped with a 532 nm laser, a 100x objective, a grating of 1800 grooves/mm and a spot size of 2 μm^2. Each spectrum was the average of 12 acquisitions, with an exposition time of 300 s for each of them. Three spectra have been collected for each

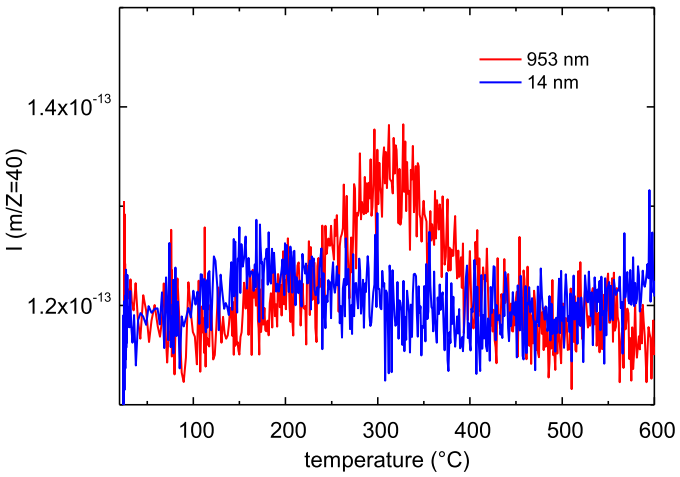

Fig. 2. Comparison of the signal of the mass spectrometer for argon gas as a function of temperature for the samples with a thickness of 14 and 953 nm.

sample on three different points (A,B,C). Since the Raman intensity can be significantly affected by small changes in the laser focus and in the sample orientation, all the spectra were rescaled and the analysis was limited to the phonon-band profiles.

Infrared and Raman spectroscopy measurements were performed on the samples with a thickness of the coating of 953 nm. As reference, the "as deposited" sample was considered and initial spectra in these conditions were acquired. Parts of the same specimen were afterwards heated up, either in air up to 500°C for 10 hours or in a vacuum of the order of 10^{-5} mbar up to 500°C for 15 hours. The spectra of samples after annealing in both conditions were further acquired, with a special care to measure in the same positions initially investigated.

3. Results

A preliminary investigation of the roughness of the surface of the samples was conducted by atomic force microscopy (AFM) topographies on the samples with thickness 4.5 and 103 nm. As reported in Fig. 1, the two Ta_2O_5 coatings exhibit an extremely flat surface with an r.m.s. roughness in the best case as low as 0.15 nm. For the 4.5 nm thick layer we observed the occurrence of some linear ditches on the surface, not observed instead in the 103 nm thick layer. The presence of these grooves is confirmed by the detection of a low Si oxide signal in XPS (see subsequent section).

Table 1
Peak energy (in eV) of the main contributions to the XPS spectra of Ta and Ar.

Element peak name	Peak energy for Ta_2O_5
Ta $4f_{5/2}$-$4f_{7/2}$	27.7-25.8
Ar 3s	24.0
Ta $4d_{3/2}$-$4d_{5/2}$	241.7-230.2
Ar $2p_{1/2}$-$2p_{3/2}$	242.0-244.0
Ta $4p_{3/2}$	404.8
Ar 2s	320.0

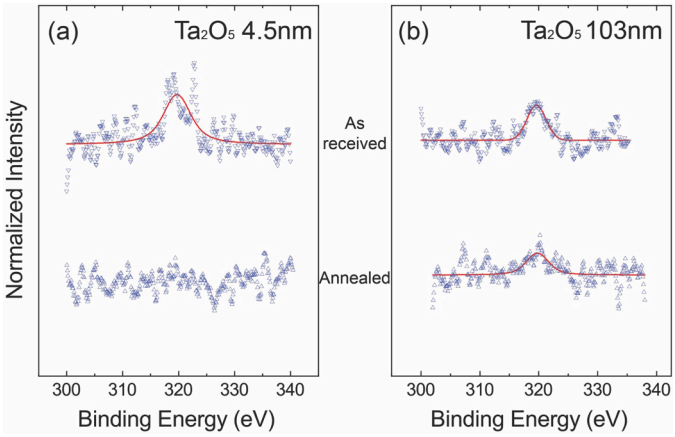

Fig. 4. XPS spectra of Ar 2s for Ta_2O_5 layers with thickness 4.5 nm (a) and 103 nm (b). Top spectra are related to the "as deposited" samples, while bottom spectra to samples after one hour annealing at 300°C in ultra-high vacuum.

In order to investigate whether some residual Argon atoms from the deposition are left in the whole coating layer or only at the interface between the substrate and the coating, we performed mass spectrometry measurements. In particular, the samples were heated in a vacuum of the order of 10^{-5} mbar in a thermobalance coupled with a quadrupole mass spectrometer. During the thermal treatment, the mass does not significantly change. Concomitantly, the mass spectrometer detects the effusion of various gaseous species. Hydrocarbons (C_nH_m) and water signals display a maximum of their intensity around 250°C, while the signal due to argon (m/Z = 40) shows a well developed peak centered around 300°C for the sample with a Ta_2O_5 coating of 953 nm; on the contrary, within the uncertainties, no clear peak is visible for the coating

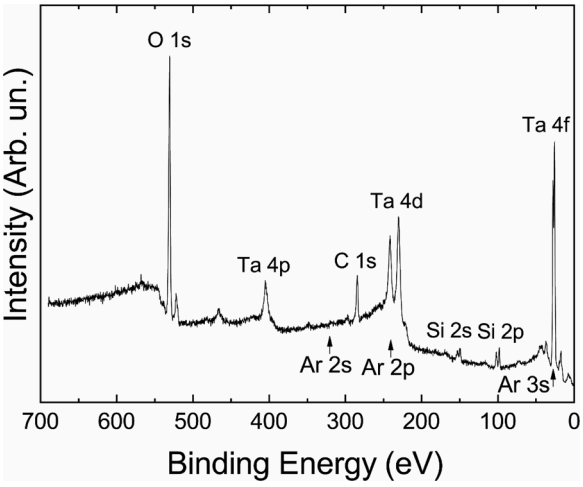

Fig. 3. XPS survey spectrum of Ta_2O_5 coating with a thickness of 4.5 nm deposited on crystalline Si.

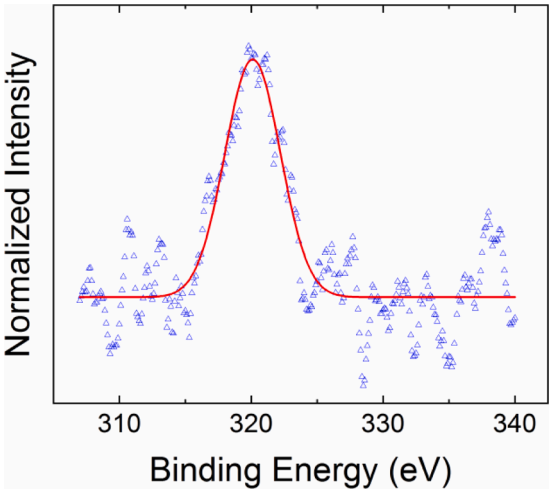

Fig. 5. XPS spectra of Ar 2s for Ta_2O_5 layers with thickness 103 nm, after annealing in air at 500°C.

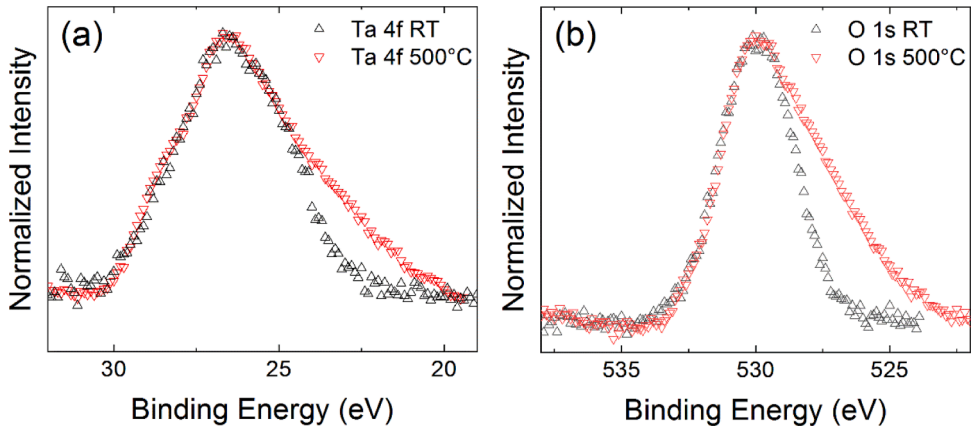

Fig. 6. XPS spectra of (a) Ta 4f, and (b) O 1s regions of Ta-oxides-based film in the as-received state and after the annealing treatment in vacuum.

of 14 nm (Fig. 2). This fact can be interpreted as the evidence that argon is present in the samples and it can be released in vacuum with a maximum of effusion around 300°C; at 500°C all the argon gas present in the specimen is discharged by means of a thermal treatment in vacuum. The negligible intensity observed for the 14 nm thick sample suggests that argon is present in the whole body of the coating, not only at the interface between Ta_2O_5 and Si. In fact, if argon came only from the interface, the intensity of the argon peak for the two thicknesses would be the same (as the surface areas of the measured samples with different thickness practically coincide). On the contrary, under the hypothesis that Ar resides in the whole coating, the intensity of the peak should scale with the ratio of the thicknesses (≈70, in the present case) and, therefore, with the sensitivity of the used mass spectrometer it should not be detectable when t=14 nm. In conclusions the mass spectrometry experiments provide evidence that argon is present in the whole amorphous Ta_2O_5 coating.

To further study the presence of Ar in the samples and its evolution with thermal treatments, X-ray photoelectron spectroscopy analysis was carried out on the samples with Ta_2O_5 coverage of 4.5 and 103 nm, respectively, both on "as-deposited" sample and after annealing; the latter either in air at 500°C (ex-situ) or in a vacuum at 300°C (in situ). The thin-coated sample was chosen in order to investigate also the

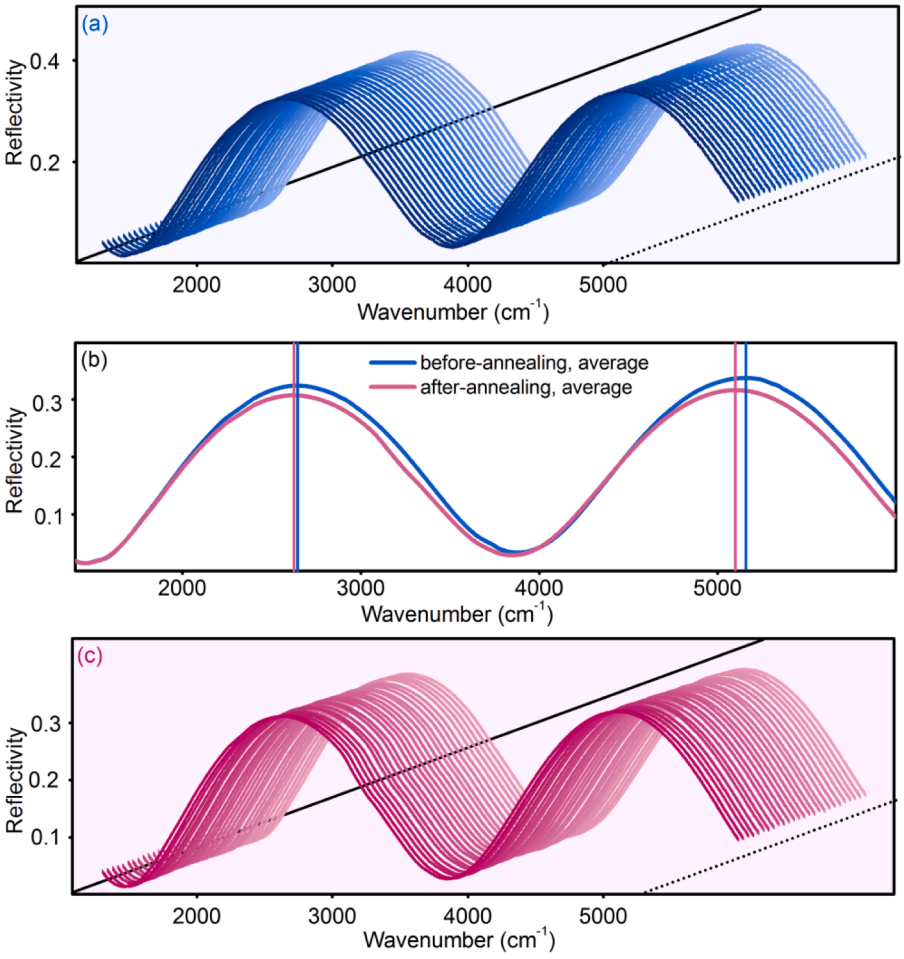

Fig. 7. (a) MIR map of "as deposited" sample before the annealing; the 25 spectra of the map are reported with different shades of blue and are shifted along the z axis. (b) Comparison between the average spectra of the sample before (blue) and after (pink) the annealing in air at 500°C; the vertical lines indicate the maxima of the curves. (c) MIR map after the annealing; the 25 spectra of the map are reported with different shades of pink and are shifted along the z axis. (For interpretation of the references to color in this figure legend, the reader is referred to the web version of this article.).

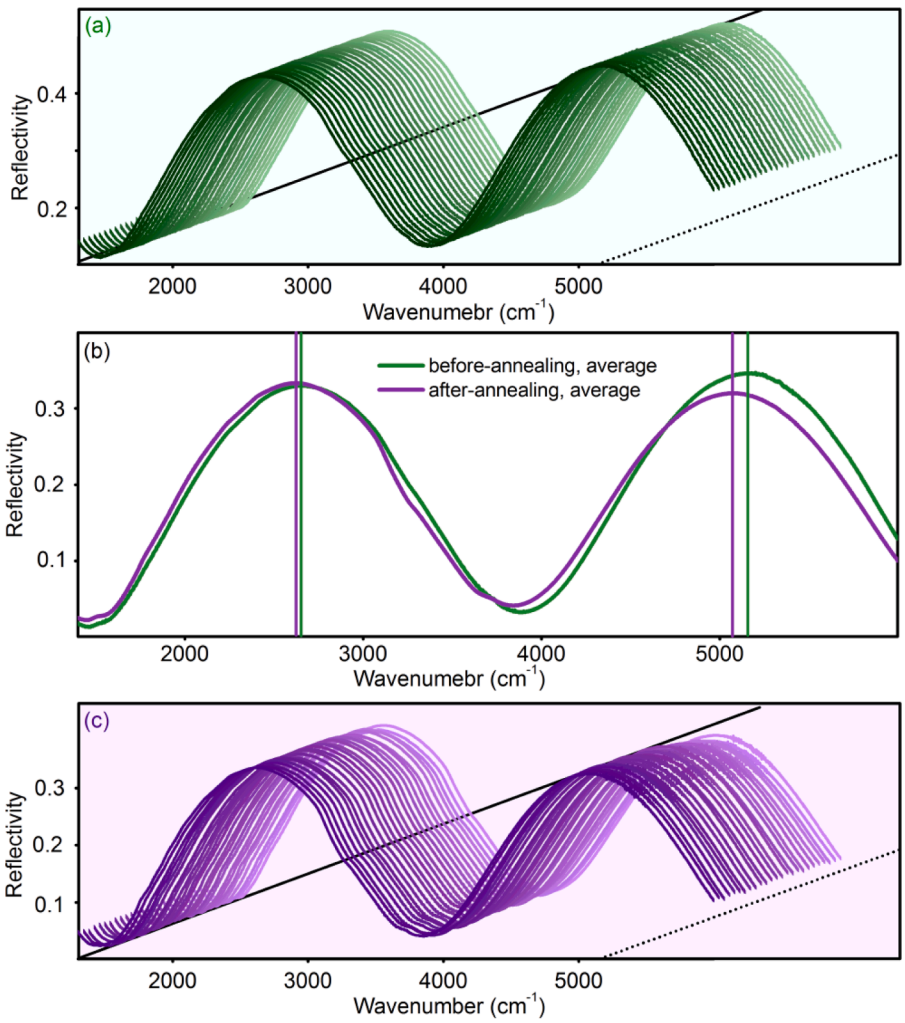

Fig. 8. (a) MIR map in the "as-deposited" state; the 25 spectra of the map are reported with different shades of green and are shifted along the z axis. (b) Comparison between the average spectra before (green) and after (purple) the annealing in vacuum at 500°C; the vertical lines indicate the maxima of the curves. (c) MIR map after the annealing; the 25 spectra of the map are reported with different shades of purple and are shifted along the z axis. (For interpretation of the references to color in this figure legend, the reader is referred to the web version of this article.).

Table 2
Maxima of the interference fringes and their period in the two wafers, before and after annealing either in air (W1) or in vacuum (W2).

Sample	1st maximum (cm^{-1})	2nd maximum (cm^{-1})	Δ_max (cm^{-1})
W1, "as-deposited"	2646	5164	2518
W1, after annealing in air	2625	5101	2476
W2, "as-deposited"	2653	5164	2511
W2, after annealing in a vacuum	2626	5074	2448

Ta_2O_5/substrate interface, thanks to the surface sensitivity of the XPS technique [21], to be compared with the thicker Ta_2O_5 sample with the deeply buried interface. The as-received sample with t=4.5 nm exhibits the characteristic XPS peaks of tantalum oxide with the expected stoichiometry (Fig. 3) and minor contributions from Ar and from Si coming from the near-surface interface (Fig. 3 and Table 1).

The Argon detection on Ta_2O_5 is not trivial since the Ar 2p peak overlaps with the Ta 4d doublet and the Ar 3s with the Ta 4f (see Table 1). The best Ar detectable peak is the 2s that exhibits a low sensitivity [22]. Nevertheless, by means of Ar 2s detection, and very long integration time, we were able to measure the presence of Ar in the Ta_2O_5 layer, as observed in Fig. 4.

The XPS spectra of the Ar 2s peak clearly point out the presence of a low percentage of Ar in the layers, estimated to less than 0.3 at.%. This small quantity remarkably reduces (by 50% for the 103 nm thick layer) or even disappears (for the 4.5 nm thick layer) after an annealing of 1 hour at 300°C in UHV conditions. In the samples annealed in air at 500°C the Ar 2s component (Fig. 5) appears reduced in intensity by only 50% with respect to the untreated samples, suggesting that the treatment in air is less effective in removing the trapped argon.

The occurrence of Ar in both samples rules out the possibility of an argon accumulation occurring only at the Ta_2O_5/Si interface and it is in agreement with indications provided by mass spectrometry. This finding is further strengthened by the behavior of Ar signal reduction under sample annealing: while argon is completed desorbed from the thin layer, we have only a partial desorption in the thick layer due to the volumetric permeation.

The thermal treatments also influence the surface stoichiometry of the thin films. We report in Fig. 6 the comparison of the Ta 4f and O 1s regions of Ta-oxides-based film in the as-received state and after the annealing in vacuum at 500°C. After the thermal treatment, different spectral components emerge in the low binding energy side of the main Ta_2O_5-associated peaks, thus suggesting a different oxidation state for tantalum, induced by heating. Specifically, on the basis of previous results [23,24], one can attribute these smaller components to the formation of different sub-stoichiometric Ta-oxides phases, namely Ta_2O_3, TaO, TaO_2, in agreement with a previous investigation performed by XPS on Ta_2O_5 thermally treated at 600°C [25]. It must be noted, however, that the change of stoichiometry is likely to be confined to the first few nm of the coating. Extensive changes in bulk stoichiometry would result in measurable changes in the Raman signal. We will show below that this is not observed.

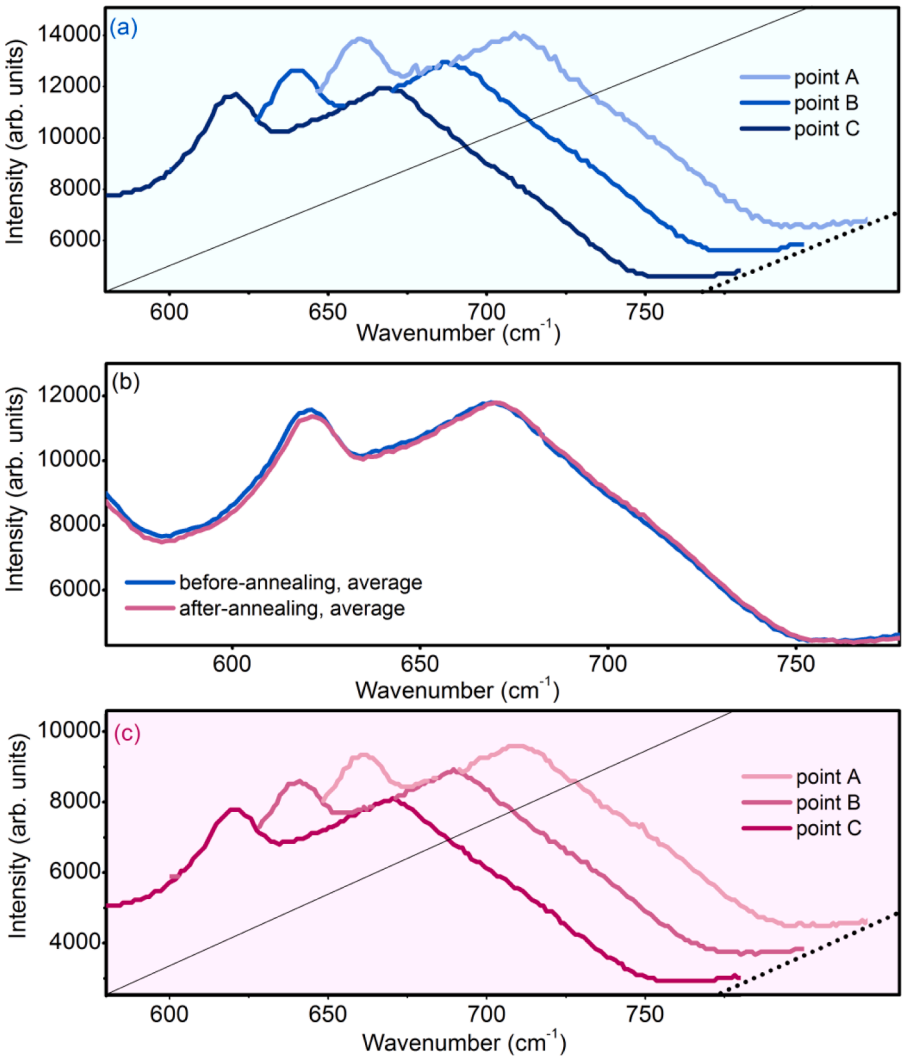

Fig. 9. (a) Raman spectra collected in three different point on w1 (A, B, C) before the annealing; the 3 spectra are reported with different shades of blue and are shifted along the z axis. (b) Comparison between the average spectra of W1 before (blue) and after (pink) the annealing in air at 500°C. (c) Raman spectra collected in three different point on W1 (A, B, C) after the annealing; the 3 spectra are reported with different shades of pink and are shifted along the z axis. (For interpretation of the references to color in this figure legend, the reader is referred to the web version of this article.).

The effects of thermal treatments on the coatings were investigated also by means of infrared and Raman spectroscopy on the samples with a coating thickness of 952 nm, in order to gain sensitivity to the coating film properties. Figs. 7 and 8 report the comparison of the infrared spectra acquired on the "as-deposited" sample and on the same sample after annealing in air (Fig. 7) or in vacuum (Fig. 8) at 500°C. In all spectra, the feature at 2300 cm^{-1} is an artefact due to atmospheric absorption.

In the infrared reflectance spectra, one can observe well defined interferences fringes, due to the superposition of the electric fields reflected at the air-Ta_2O_5 and at the Ta_2O_5-Si interfaces, respectively. The period of these fringes is given by $(nd)^{-1}$, being n the real refractive index of Ta_2O_5 and d the optical path of the radiation within the Ta_2O_5 film. Table 2 displays the period of the fringes calculated for each sample before and after annealing either in air (W1) or in vacuum (W2).

As shown in Table 2, before the annealing, the spacing of the fringes, Δ_max, is almost the same for the two samples, W1 and W2 (2518 and 2511 cm^{-1}, respectively); after the annealing, the fringe spacing Δ_max reduces for both samples, although the decrease is significantly larger in the sample annealed in vacuum (63 cm^{-1}) than in the one thermally treated in air (42 cm^{-1}). We can conclude that in both wafers the annealing affects the dn product, but in the sample annealed in vacuum this effect is more evident. Infrared spectroscopy cannot separate the contribution from the refractive index or the coating thickness to the modulation of the fringes. However, previous measurements on amorphous Ta_2O_5 deposited on SiO_2 substrates indicated that n lightly decreases after thermal treatments [16,26]. Therefore, in the present case, the thickness of the coating films should increase after annealing by ~15-20 nm in the two samples (~1-2%). Such increase of the coating thickness was also suggested by previous spectroscopic ellipsometry measurements on Ta_2O_5 films deposited on silica substrates [26] and interpreted as due to an increase of the volume of the pores present in the structure upon annealing [26].

It must be noted, however, that no major changes of the macroscopic structure of Ta_2O_5 occur during the annealing, either in vacuum or in air. In fact, Figs. 9 and 10 display the comparison of the Raman spectra of samples W1 and W2 (the same measured by infrared spectroscopy) before and after the annealing in air or in vacuum. The two peaks at ~620 and ~640 cm^{-1} can be attributed to silicon oxide, while the underlying band between 600 and 750 cm^{-1} has been assigned to amorphous Ta_2O_5 by comparison with the literature [27]. It can be noted (Figs. 9 and 10) that not only the oxide band-profile does not depend on the position on the sample (Figs. 9a, 9d, 10a, 10d), but it remains also unchanged before and after the annealing procedures (Figs. 9c, 10c), thus ensuring a good homogeneity of the sample on the micrometer scale.

4. Conclusions

The present study investigated the effects of thermal treatments in

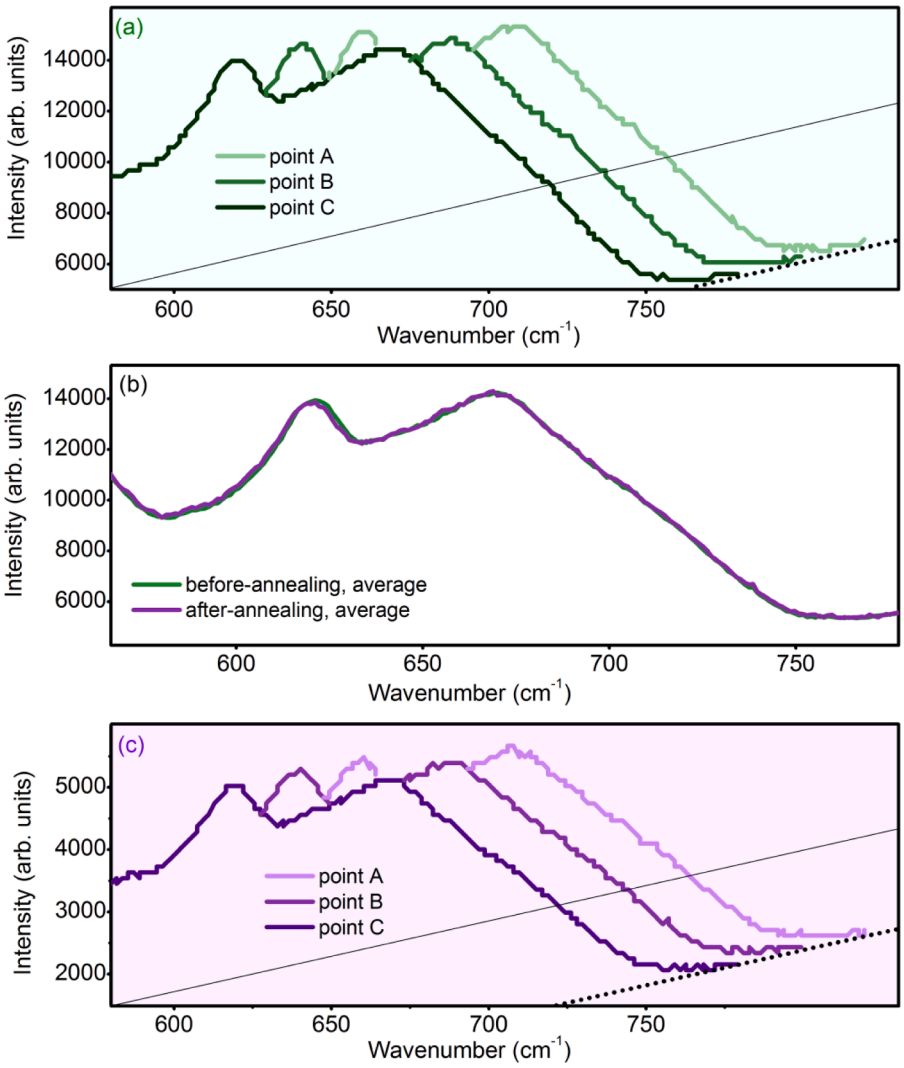

Fig. 10. (a) Raman spectra collected in three different point on W2 (A, B, C) before the annealing; the 3 spectra are reported with different shades of green and are shifted along the z axis. (b) Comparison between the average spectra of W2 before (green) and after (purple) the annealing in vacuum. (c) Raman spectra collected in three different point on W2 (A, B, C) afterthe annealing; the 3 spectra are reported with different shades of purple and are shifted along the z axis. (For interpretation of the references to color in this figure legend, the reader is referred to the web version of this article.).

vacuum or in air on amorphous Ta_2O_5 deposited on crystalline Si, mimicking the mirrors of gravitational-wave detectors. Evidence is provided that the synthesis by Ion Beam Sputtering leaves some argon atoms (less than 0.3 at%) inside the whole thickness of the Ta_2O_5 film. Argon is released when the sample is heated in vacuum above 200°C, however it remains entrapped in the sample if the annealing is conducted in air, even at temperatures as high as 500°C. The macroscopic structure of the samples is not strongly affected by heating; however, some substoichiometric Ta oxides develop on the surface of the coating after heating in vacuum. Finally, the thickness of the Ta_2O_5 seems to increase by ~1-2% after annealing, due to the increase of the size of the pores present in the coating.

Credit author

Conceptualization G. Cagnoli, E. Majorana, F. Ricci

Methodology Development A. Paolone, E. Placidi, E. Stellino, M. G. Betti, E. Majorana, C. Mariani, A. Nucara, O. Palumbo, P. Postorino, I. Rago, F. Trequattrini, F. Ricci

Validation A. Paolone, E. Placidi, E. Stellino, M. G. Betti, E. Majorana, C. Mariani, A. Nucara, O. Palumbo, P. Postorino, I. Rago, F. Trequattrini, F. Ricci

Formal analysis A. Paolone, E. Placidi, E. Stellino, M. G. Betti, C. Mariani, A. Nucara, O. Palumbo, P. Postorino, I. Rago, F. Trequattrini, F. Ricci

Investigation A. Paolone, E. Placidi, E. Stellino, M. G. Betti, E. Majorana, C. Mariani, A. Nucara, O. Palumbo, P. Postorino, I. Rago, F. Trequattrini, F. Ricci

Resources M. Granata, J. Teillon, D. Hofman, C. Michel, A. Lemaitre, N. Shcheblanov

Writing - Original Draft A. Paolone

Writing - Review & Editing All authors

Visualization A. Paolone, E. Placidi, E. Stellino, M. G. Betti, E. Majorana, C. Mariani, A. Nucara, O. Palumbo, P. Postorino, I. Rago, F. Trequattrini, F. Ricci

Supervision G. Cagnoli, A. Paolone, F. Ricci

Funding acquisition G. Cagnoli, M. G. Betti, E. Majorana, A. Paolone, F. Ricci

Declaration of Competing Interest

The authors declare that they have no known competing financial interests or personal relationships that could have appeared to influence the work reported in this paper.

Acknowledgments

The present work has been performed in the framework of the Virgo Coating Research and Development collaboration. The support of Sapienza Grande Progetto di Ateneo 2017, Amaldi Research Center

(MIUR program "Dipartimento di Eccellenza" CUP:B81I18001170001), of European Gravitational Observatory and of Istituto Nazionale di Fisica Nucleare is gratefully acknowledged. We wish to thank S. Brutti for the use of one of his furnaces for some thermal treatments.

References

[1] C. Li, F. Wang, K. Hu, W. Li, J. Zhao, T. Ren, Z. Song, K. Zhang, Ultralow power switching of Ta_2O_5/AlO_X bilayer synergistic resistive random access memory, J. Phys. D 53 (2020), 335104, https://doi.org/10.1088/1361-6463/ab8b02.

[2] L. Splitthoff, M.A. Wolff, T. Grottke, C. Schuck, Tantalum pentoxide nanophotonic circuits for integrated quantum technology, Opt. Express 28 (2020) 11921–11932, https://doi.org/10.1364/OE.388080.

[3] B. Liu, W. Liu, New room temperature ammonia gas sensor synthesized by a tantalum pentoxide (Ta_2O_5) dielectric and catalytic platinum (Pt) metals, IEEE Trans. Electron Devices 67 (2020) 2566–2572, https://doi.org/10.1109/TED.2020.2986795.

[4] F. Magesa, Y. Wu, S. Dong, Y. Tian, G. Li, J.M. Vianney, J. Buza, J. Liu, Q. He, Electrochemical sensing fabricated with Ta_2O_5 nanoparticle-electrochemically reduced graphene oxide nanocomposite for the detection of oxytetracycline, Biomolecules 10 (2020) 110, https://doi.org/10.3390/biom10010110.

[5] L. Yang, Y. Yang, J.R. Lombardi, Y. Peng, Z. Huang, Charge transfer enhancement in the surface-enhanced Raman scattering of Ta_2O_5 superstructures, Appl. Surf. Sci. 520 (2020), 146325, https://doi.org/10.1016/j.apsusc.2020.146325.

[6] W.-S. Liu, M.-W. Liao, S.-H. Huang, Y.I.A. Reyes, H.-Y.T. Chen, T.-P. Perng, Formation and characterization of gray Ta_2O_5 and its enhanced photocatalytic hydrogen generation activity, Int. J. Hydrog. Energy 45 (2020) 16560–16568, https://doi.org/10.1016/j.ijhydene.2020.04.154.

[7] N. Sharma, V.S.R.S. Praveen Kumar, M. Kumar, N. Kumari, V. Karar, J. K. Goswamy, A.L. Sharma, Fabrication and estimation of optical constants of hydrophobic Ta_2O_5 thin films, Optik 202 (2020), 163697, https://doi.org/10.1016/j.ijleo.2019.163697.

[8] A. Amato, G. Cagnoli, M. Canepa, E. Coillet, J. Degallaix, V. Dolique, D. Forest, M. Granata, V. Martinez, C. Michel, L. Pinard, B. Sassolas, J. Teillon, High-reflection coatings for gravitational-wave detectors: state of the art and future developments, J. Phys. 957 (2018), 012006, https://doi.org/10.1088/1742-6596/957/1/012006.

[9] M. Granata, L. Balzarini, J. Degallaix, V. Dolique, R. Flaminio, D. Forest, D. Hofman, C. Michel, R. Pedurand, L. Pinard, B. Sassolas, N. Straniero, J. Teillon, G. Cagnoli, Internal friction and Young's modulus measurements on SiO_2 and Ta_2O_5 films done with an ultra-high Q silicon-wafer suspension, Archi. Metall. Mater. 60 (2015) 365–370, https://doi.org/10.1515/amm-2015-0060.

[10] J. Steinlechner, I.W. Martin, J. Hough, C. Krüger, S. Rowan, R. Schnabel, Thermal noise reduction and absorption optimization via multimaterial coatings, Phys. Rev. D 91 (2015), 042001, https://doi.org/10.1103/PhysRevD.91.042001.

[11] M. Granata, E. Saracco, N. Morgado, A. Cajgfinger, G. Cagnoli, J. Degallaix, V. Dolique, D. Forest, J. Franc, C. Michel, L. Pinard, R. Flaminio, Mechanical loss in state-of-the-art amorphous optical coatings, Phys. Rev. D 93 (2016), 012007, https://doi.org/10.1103/PhysRevD.93.012007.

[12] M.R. Abernathy, X. Liu, T.H. Metcalf, An overview of research into low internal friction optical coatings by the gravitational wave detection community, Mat. Res. 21 (suppl.2) (2018), e20170863, https://doi.org/10.1590/1980-5373-mr-2017-0863.

[13] A. Amato, S. Terreni, V. Dolique, D. Forest, G. Gemme, M. Granata, L. Mereni, C. Michel, L. Pinard, B. Sassolas, J. Teillon, G. Cagnoli, M. Canepa, Optical properties of high-quality oxide coating materials used ingravitational-wave advanced detectors, J. Phys. 2 (2019), 035004, https://doi.org/10.1088/2515-7639/ab206e.

[14] F. Acernese, et al., VIRGO collaboration, status of advanced virgo, EPJ Web Conf. 182 (2018) 02003, https://doi.org/10.1051/epjconf/201818202003.

[15] F. Acernese, et al., VIRGO collaboration, advanced virgo status, J. Phys. 1342 (2020), 012010, https://doi.org/10.1088/1742-6596/1342/1/012010.

[16] M. Granata, A. Amato, L. Balzarini, M. Canepa, J. Degallaix, D. Forest, V. Dolique, L. Mereni, C. Michel, L. Pinard, B. Sassolas, J. Teillon, G. Cagnoli, Amorphous optical coatings of present gravitational-wave interferometers, Class. Quantum Grav. 37 (2020), 095004, https://doi.org/10.1088/1361-6382/ab77e9.

[17] G.M. Harry, M.R. Abernathy, A.E. Becerra-Toledo, H. Armandula, E. Black, K. Dooley, M. Eichenfield, C. Nwabugwu, A. Villar, D.R.M. Crooks, G. Cagnoli, J. Hough, C.R. How, I. MacLaren, P. Murray, S. Reid, S. Rowan, P.H. Sneddon, M. M Fejer, R. Route, S.D. Penn, P. Ganau, J.-M. Mackowski, C. Michel, L. Pinard, A. Remillieux, Titania-doped tantala/silica coatings for gravitational-wave detection, Class. Quant. Grav. 24 (2007) 405–416, https://doi.org/10.1088/0264-9381/24/2/008.

[18] R. Bassiri, F. Liou, M.R. Abernathy, A.C. Lin, N. Kim, A. Mehta, B. Shyam, R. L. Byer, E.K. Gustafson, M. Hart, I. MacLaren, I.W. Martin, R.K. Route, S. Rowan, J. F. Stebbins, M.M. Fejer, Order within disorder: the atomic structure of ion-beam sputtered amorphous tantala (a-Ta_2O_5), APL Materials 3 (2015), 036103, https://doi.org/10.1063/1.4913586.

[19] M.J. Hart, R. Bassiri, K.B. Borisenko, M. Véron, E.F. Rauch, I.W. Martin, S. Rowan, M.M. Fejer, I. MacLaren, Medium range structural order in amorphous tantala spatially resolved with changes to atomic structure by thermal annealing, J. Non-Cryst. Solids 438 (2016) 10–17, https://doi.org/10.1016/j.jnoncrysol.2016.02.005.

[20] O. Palumbo, A. Paolone, P. Rispoli, R. Cantelli, T. Autrey, Decomposition of NH_3BH_3 at sub-ambient pressures: a combined thermogravimetry–differential thermal analysis–mass spectrometry study, J. Power Sources 195 (2010) 1615–1618, https://doi.org/10.1016/j.jpowsour.2009.09.042.

[21] A. Paolone, M. Angelucci, S. Panero, M.G. Betti, C. Mariani, Thermal stability and reduction of iron oxide nanowires at moderate temperatures, Beilstein J. Nanotechnol. 5 (2014) 323–328, https://doi.org/10.3762/bjnano.5.36.

[22] J.J. Yeh, I. Lindau, Atomic subshell photoionization cross sections and asymmetry parameters: $1 \leqslant Z \leqslant 103$, At. Data Nucl. Data Tables 32 (1985) 1–155, https://doi.org/10.1016/0092-640X(85)90016-6.

[23] E Atanassova, G Tyuliev, A Paskaleva, D Spassov, K Kostov, XPS study of N_2 annealing effect on thermal Ta_2O_5 layers on Si, Appl. Surf. Sci. 225 (2004) 86–99, https://doi.org/10.1016/j.apsusc.2003.09.040.

[24] I. Perez, V. Sosa, F. Gamboa, J.T.E. Galindo, J.L. Enríquez-Carrejo, R. Farías, P. G. Mani González, Influence of post-deposition annealing on the chemical states of crystalline tantalum pentoxide films, Appl. Phys. A 124 (2018) 792, https://doi.org/10.1007/s00339-018-2198-9 (2018).

[25] M. Prato, E. Cesarini, M. Lorenzini, A. Chincarini, G. Cagnoli, M. Canepa, F. Vetrano, G. Gemme, Multitechnique investigation of Ta_2O_5 films on SiO_2 substrates: comparison of optical, chemical andmorphological properties, J. Phys. 228 (2010), 012020, https://doi.org/10.1088/1742-6596/228/1/012020.

[26] L. Anghinolfi, M. Prato, A. Chtanov, M. Gross, A. Chincarini, M. Neri, G. Gemme, M. Canepa, Optical properties of uniform, porous, amorphous Ta_2O_5 coatings on silica: temperature effects, J. Phys. D 46 (2013), 455301, https://doi.org/10.1088/0022-3727/46/45/455301.

[27] C. Joseph, P. Bourson, M.D. Fontana, J. Raman Spectr. 43 (2012) 1146–1150, https://doi.org/10.1002/jrs.3142.